Title	Macrospin and micromagnetic studies of tilted polarizer spin-torque nano-oscillators
Author(s)	Zhou, Y; Zhang, H; Liu, Y; Åkerman, J
Citation	Journal Of Applied Physics, 2012, v. 112 n. 6, article no. 063903
Issued Date	2012
URL	http://hdl.handle.net/10722/159785
Rights	Creative Commons: Attribution 3.0 Hong Kong License

AIP | Journal of Applied Physics

Macrospin and micromagnetic studies of tilted polarizer spin-torque nano-oscillators

Yan Zhou, Hong Zhang, Yaowen Liu, and Johan Åkerman

Citation: J. Appl. Phys. **112**, 063903 (2012); doi: 10.1063/1.4752265
View online: http://dx.doi.org/10.1063/1.4752265
View Table of Contents: http://jap.aip.org/resource/1/JAPIAU/v112/i6
Published by the American Institute of Physics.

Macrospin and micromagnetic studies of tilted polarizer spin-torque nano-oscillators

Yan Zhou,[1,a)] Hong Zhang,[2] Yaowen Liu,[2] and Johan Åkerman[3,4]
[1]*Department of Physics, The University of Hong Kong, Hong Kong*
[2]*Department of Physics, Tongji University, Shanghai 200092, China*
[3]*Physics Department, University of Gothenburg, 412 96 Gothenburg, Sweden*
[4]*Materials Physics, School of Information and Communication Technology, KTH-Royal Institute of Technology, Electrum 229, 164 40 Kista, Sweden*

(Received 30 May 2012; accepted 9 August 2012; published online 17 September 2012)

Using nonlinear dynamical systems theory, we analytically studied a spin-torque device in which the magnetization of the polarizer (the fixed layer) is tilted at an arbitrary angle out of the thin-film plane. While the analytical theory can determine the major features of the system, macrospin simulations were employed to demonstrate the unique characteristics of the system, such as the hysteretic switching between bistable states. Material dependencies of the dynamic and static state diagrams were also studied in the framework of the macrospin model. Full-scale micromagnetics simulations were finally performed to reveal more subtle features of the dynamics of such tilted polarizer systems. Both the macrospin and micromagnetics simulations gave quantitatively the same results as our analytical theory. © *2012 American Institute of Physics*. [http://dx.doi.org/10.1063/1.4752265]

I. INTRODUCTION

A spin-torque nano-oscillator (STNO) is a nanosized device capable of microwave generation in almost the entire Gigahertz range.[1–6] STNOs have the advantages of a wide tunability range,[7] very high modulation rates,[3,8–10] compact device size, and the same high compatibility with standard CMOS process as magnetoresistive random access memory (MRAM),[11,12] making the device very promising for potential microwave generation and wireless communication applications.[1–6] However, some challenges need to be solved before this technology can find practical application. The two most important roadblocks are low output power (on the order of 1 μW for a single device) and the need for an applied magnetic field for operation. To solve the power limitation problem, two solutions have been proposed, namely, (a) improving the magnetoresistance (MR) of a single device by optimizing the material properties and device fabrication,[13,14] and (b) synchronizing a series of STNOs to produce enhanced phase-coherent microwave oscillation.[5,15–21] Additionally, various efforts have been made to remove the applied magnetic field, which typically ranges from a few hundred Oersteds to over 1 T. The most widely adopted zero-field operation approaches include STNOs with a perpendicularly magnetized fixed[22] or free layer,[23,24] vortex oscillators,[25–30] wavy-torque spin-torque oscillators,[31] and tilted-polarizer STNOs (TP-STNOs).[32–37]

A TP-STNO is a nanosized spintronic device, where the magnetization of the fixed layer is tilted with respect to the film plane.[32,33] In such a structure, the tilted spin polarization has both an in-plane component and an out-of-plane component. This can either be achieved using materials with a strong tilted magnetocrystalline anisotropy[38–40] or exchange springs where the competition between a layer with perpendicular magnetic anisotropy and another with in-plane anisotropy allows for a tunable magnetization angle.[41,42] The out-of-plane component of the spin-polarized current can drive the free layer into steady precession under *zero* applied magnetic field, while the in-plane component of the fixed-layer magnetization generates a large MR without the need for an additional read-out layer. Since our first report on TP-STNOs, intense interest has been generated in studying such TP-STNO-based devices.[36,37,43–46] The tilted polarizer of the fixed-layer magnetization brings a new degree of freedom into the system. While the design of such a TP device and its initial experimental fabrication have been studied in our earlier work,[32,33,39,40] a detailed study—especially a full-scale micromagnetics study—of the effects of the tilted polarizer on the dynamics of the TP device is still lacking.

In this work, we first constructed the phase diagram of the TP-STNO as a function of the applied current and tilt angle, using both the analytical theory and the macrospin approach. Full scale micromagnetic simulations were then performed for comparison with the analytical theory. We believe such a multiscale study to be important in understanding the unique physical characteristics of this type of device, and may provide useful guidelines to optimize the output of such TP devices.

The paper is organized as follows: In Sec. II, a theoretical model is developed to construct the phase diagram of the TP device. Macrospin simulations are performed to study the dependence of the phase diagram on various material parameters. In Sec. III, we perform micromagnetics simulations of a TP-STNO and compare our results with analytical theory and macrospin model. Finally, a brief summary of the main results is given in Sec. IV.

II. EIGENVALUE ANALYSIS AND THE MACROSPIN MODEL

The schematic structure of the TP device is illustrated in Fig. 1. In the framework of the macrospin model, the time evolution of the unit vector of the free-layer magnetization

[a)]Electronic address: yanzhou@hku.hk.

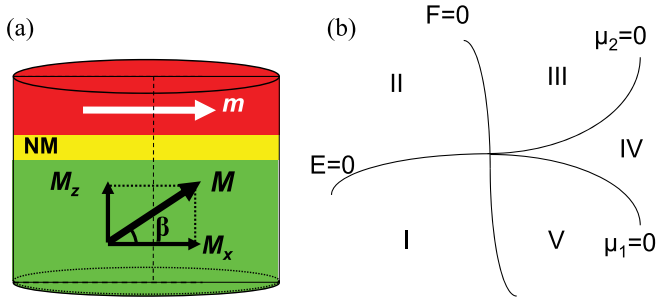

FIG. 1. (a) The proposed tilted-polarizer device structure. **m** and **M** are the magnetization vectors of the free and fixed layers, respectively. **M** lies in the *x*-*z*, plane with angle β with respect to the *x*-axis. Here, the *x*-*y* plane is the easy plane (the film plane), with the *x*-axis being the easy axis. (b) Schematic representation of the device's switching phase diagram.

$\hat{m}$ follows the Landau-Lifshitz-Gilbert-Slonczewski (LLGS) equation,[47,48]

$$\frac{d\hat{m}}{dt} = -|\gamma|\hat{m} \times \mathbf{H}_{eff} + \alpha\hat{m} \times \frac{d\hat{m}}{dt} + |\gamma|\alpha_J\hat{m} \times (\hat{m} \times \hat{M}), \quad (1)$$

and the last term is the Slonczewski spin torque with magnitude

$$\alpha_J = \frac{\hbar\xi(1+\chi)J}{ed\mu_0 M_s[2+\chi(1+\cos\varphi)]}, \quad (2)$$

where γ is the gyromagnetic ratio, α is the Gilbert damping parameter, μ_0 is the magnetic vacuum permeability, M_s is the free-layer saturation magnetization, $\hbar$ is the reduced Planck constant, d the free-layer thickness, e the electron charge, and J the electric current density. ξ is the spin-polarization efficiency constant. χ is the giant magnetoresistance (GMR) asymmetry parameter, describing the deviation from sinusoidal angular dependence. φ is the angle between $\hat{m}$ and $\hat{M}$.

The applied field H_{app} is set to zero throughout this work, since we consider the spin-torque driven magnetization dynamics only. By decomposing the demagnetizing tensor, the effective field can be expressed as $\mathbf{H}_{\text{eff}} = (H_k\hat{e}_x m_x - H_d\hat{e}_z m_z)/|\mathbf{m}|$, where H_k is the positive shape anisotropy field along the *x*-axis (the easy-axis), and H_d is the out-of-plane demagnetization field (the easy-plane anisotropy) in the direction perpendicular to the plane (the *z*-axis). The electric current is defined as positive when it flows from the fixed to the free layer, and is normalized by $J_0 = 10^8\,\text{A/cm}^2$. For the results presented here, $|\gamma| = 1.9 \cdot 10^{11}\,\text{Hz/T}$, $\mu_0 H_k = 10^{-2}\,\text{T}$, $\xi = 0.35$, and $\chi = 0$.[25,33] The lateral dimension of the NiFe thin-film free layer is assumed to be an elliptical shape of 130 nm × 70 nm, with a thickness of 3 nm. The thickness of the FePt fixed layer is 20 nm.

Equation (1) can be transformed into the following set of differential equations in spherical coordinates:

$$\begin{aligned}\Gamma\dot{\theta} &= \frac{\sin(2\theta)H_d\alpha}{2} + [\cos^2\phi\sin(2\theta)\alpha - \sin(2\phi)\sin(\theta)]\frac{H_k}{2} \\ &\quad -(M_\theta - \alpha M_\phi)\alpha_J, \\ \Gamma\dot{\phi} &= -\cos(\theta)H_d\alpha - [2\cos^2\phi\cos(\theta) - \alpha\sin(2\phi)]\frac{H_k}{2} \\ &\quad -\csc(\theta)(\alpha M_\theta + M_\phi)\alpha_J, \end{aligned} \quad (3)$$

with $M_\theta = M(\cos\beta\cos\theta\cos\phi - \sin\beta\sin\theta), M_\phi = -M\cos\beta\sin\phi$, and $\Gamma \equiv (1+\alpha^2)|\gamma|^{-1}$.

The equilibrium solutions of Eq. (3) are: $\bar{\theta}_i = \bar{\theta}_i(\beta, J)$, $\bar{\phi}_i = \bar{\phi}_i(\beta, J)$, where $i \le i_t$ is the ith solution of the total i_t solutions. However, only some of these i_t equilibrium states are stable. Equation (3) can be linearized in the vicinity of $(\bar{\theta}_i, \bar{\phi}_i)$

$$\begin{bmatrix}\dot{\theta}\\ \dot{\phi}\end{bmatrix} = \begin{bmatrix}A(\beta,J,\bar{\theta}_i,\bar{\phi}_i) & B(\beta,J,\bar{\theta}_i,\bar{\phi}_i)\\ C(\beta,J,\bar{\theta}_i,\bar{\phi}_i) & D(\beta,J,\bar{\theta}_i,\bar{\phi}_i)\end{bmatrix} \cdot \begin{bmatrix}\hat{\theta}\\ \hat{\phi}\end{bmatrix}. \quad (4)$$

Here A, B, C, and D are explicit functions of the variables β, J, and the other material parameters. The stability of the system can be determined by means of the eigenvalues of the corresponding Jacobian,[49] and can therefore be solved and expressed as $\mu_{1,2} = E(\beta,J) \pm \sqrt{F(\beta,J)}$ with $E = \frac{A+D}{2}$, and $F = \frac{[A+D]^2 - 4BC}{4}$. A stable solution must satisfy $\Re\{\mu_{1,2}\} < 0$. For real eigenvalues and $F > 0$, the eigenvalue with larger magnitude dominates, and defines the only eigenvector governing the approach towards the final state, in this case a node (*N*). For $F = 0$, the two eigenvectors are identical and again define a node. For $F < 0$, the complex conjugate eigenvalues define two complex eigenvectors generating an oscillatory trajectory towards equilibrium, characteristic of a spiral-like (S) solution.[50] In addition, in regions where there are neither *S* nor *N* solutions, we can infer that steady precession (*L*) must take place according to the Poincare-Bendixson theorem.[51–55]

An illustrative switching diagram is shown in Fig. 1(b). Two important lines in the (β, J) parameter space are defined by the equations $E(\beta,J) = 0$ and $F(\beta,J) = 0$. In the $F < 0$ domain, the eigenvalues are complex conjugate. Here, crossing the $E = 0$ line means changing the nature of the focus between stable and unstable. In the $F > 0$ region, both eigenvalues are real, and although the $E = 0$ line is here irrelevant, two additional lines emerge: $\mu_1 = E + \sqrt{F} = 0$ and $\mu_2 = E - \sqrt{F} = 0$. They divide the $F > 0$ domain of the parameter space into three regions in which the equilibrium is a stable focus, an unstable focus, or a saddle.[56]

Following this procedure, we now construct the static part of the phase diagram in Fig. 2 by finding all the eigenvalues in the parameter space $0° < \beta < 90°$ and $|J/J_0| < 10$. The details of the construction of Fig. 2(a) have been published in our earlier paper.[34] In addition to the analytical theory, we also performed a macrospin simulation. As shown in the inset of Fig. 2(a), if the initial configuration of the free-layer magnetization starts within the brown-colored region on the unit sphere, then it will relax in a direct way to N, as delineated by the green curve (three examples are shown here). In contrast, if the initial state of free-layer magnetization falls within the blue region, it will develop a spiral trajectory toward the final state, labeled S, as denoted by the yellow curve. This clearly shows that the evolution of the trajectory and the final static state of the magnetization depend on the initial condition for the same set of parameters. This is a typical feature of nonlinear systems, and such dependence cannot be solved by means of analytical theory. Instead, numerical simulations must be performed in order to completely reveal all the eigenstates of the system.[18–20] This also facilitates our understanding of the coexisting regions,

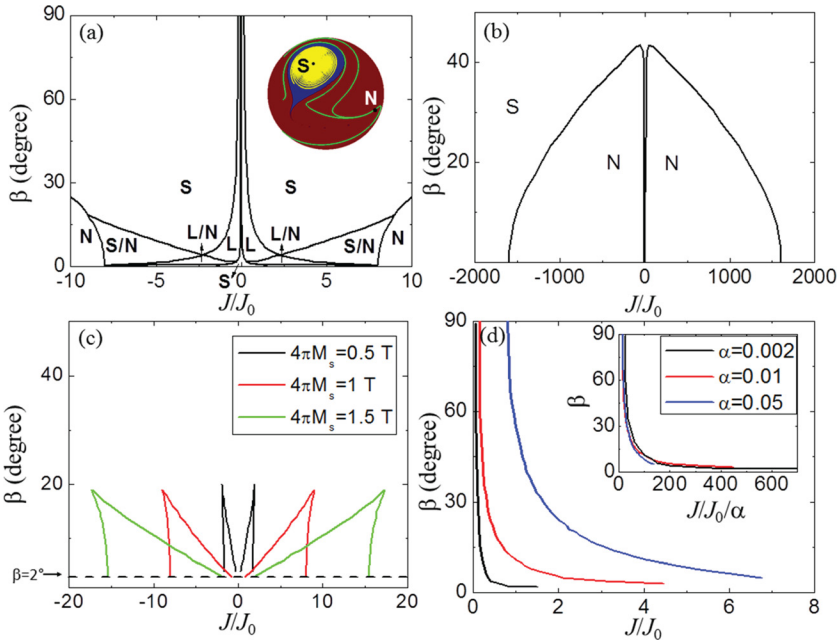

FIG. 2. (a) Analytical phase diagram of the structure of the TP device for small to medium electric current, i.e., $|J| \leq 10\,|J_0|$. The inset shows the dependence of the final static states on the initial condition. (b) Analytical phase diagram for the TP device in the high-J region, $|J| \leq 2000\,|J_0|$. (c) Effect of the free-layer saturation magnetization M_S on the boundary of the S/N region of the phase diagram from Fig. 2(a). (d) The effect of the damping coefficient α on the oscillatory region (L) of the phase diagram in (a). Here, for simplicity, only the region of positive J is shown. Inset is the plot of the oscillatory region dependence on β and $J/J_0/\alpha$.

such as L/N and S/N, which appear in the analytical phase diagram. These bistable regions correspond to hysteretic switching between different static states and between static and dynamic states. For example, if the initial magnetization state starts with $\beta = 3^\circ$ and $J = -10 \times 10^8\,\mathrm{A/cm^2}$ in the N region, then that N state will extend all the way to the L/N-L boundary as J increases. However, if we start from an initial L state with $\beta = 3^\circ$ and $J = -0.8 \times 10^8\,\mathrm{A/cm^2}$, then the L state will extend down to the boundaries of S/N and L/N, and will develop into the S state until it reaches the boundary of the S/N-N regions, as the current decreases. While Fig. 2(a) shows the state diagram for the moderate-J region of the experimentally accessible range, the S/N boundary for the extremely high-J regime ($|J/J_0| < 2000$) is shown only for completeness. By means of macrospin simulations, we can also study the dependence of the state diagram on the various material parameters. Fig. 2(c) illustrates the impact of different saturation magnetizations of the free layer (M_s) on the boundary of the S/N coexistence regime in the calculated phase diagram shown in Fig. 2(a). The dashed line delineates the onset of the coexistence region as β increases for a given J. It can be seen that the boundary shifts to the larger J value as M_s gradually increases. This is due to the counterbalancing of the demagnetization torque (proportional to M_s) with the spin-transfer torque (proportional to J). The effect of the damping constant α on the precessional regime of the TP device is shown in Fig. 2(d). Here, it can be seen that α affects the precessional states of the device, and the boundary of the limit cycle will shift to a larger J value with increasing α. Interestingly, if we plot the oscillatory region as a function of β and $J/J_0/\alpha$, then the three curves almost overlap (see the inset of Fig. 2). This can be easily understood since the limit cycle can only be sustained when the spin transfer torque, which is proportional to current density J/J_0 as denoted by the last term in the right hand side of Eq. (1), counterbalances the damping torque (the second term in the RHS of Eq. (1)) which is proportional to α. Thus, the three curves almost fall on one another. In addition, we have checked the effect of α on the equilibrium states of the device, and observed that the boundary of the N/S region does not change with α. This can be understood by examining the LLGS equation, Eq. (1). The system will be independent of α when $d\hat{m}/dt$ is set to zero.

III. MICROMAGNETICS SIMULATIONS

In order to verify our theory and the macrospin simulations, we also carried out micromagnetic simulations capable of providing detailed information on the dynamics of the magnetization precession. The micromagnetics package was developed in-house by the co-authors, and includes the spin-transfer torque terms.[57,58] Fig. 3 shows the two typical precessions of the averaged magnetization for S and N states at electric current values of $J = 0.2 \times 10^8\,\mathrm{A/cm^2}$ and $2 \times 10^8\,\mathrm{A/cm^2}$ for $\beta = 10^\circ$. The current density and tilt angle are taken from the regime of the S state and the N state, respectively, as shown in Fig. 2. The initial magnetization configuration is along the +x direction. In Fig. 3(a), after applying the current, the spin torque first drives the magnetization spiral away from the initial +x, with an increasing angle of precession. The precession state is unstable and eventually switches to the −x direction. For a large current of $2 \times 10^8\,\mathrm{A/cm^2}$, the magnetization directly switches from the +x to the −x direction without any spiral precession, on account of the strong in-plane spin torque: see Fig. 3(b).

Fig. 4(a) shows a typical L steady precession state at $J = 0.7 \times 10^8\,\mathrm{A/cm^2}$ and a tilt angle of $\beta = 10^\circ$. In this case, a large-angle precession state of magnetization along the +z axis is excited, in which the out-of-plane component of the spin torque plays a dominant role. The spin torque is balanced by the damping torque, leading to a stable cycle of precession states. The corresponding frequency spectrum shows a sharp peak with a linewidth of 400 MHz—see Fig. 4(b). By keeping $\beta = 10^\circ$ and increasing the electric current

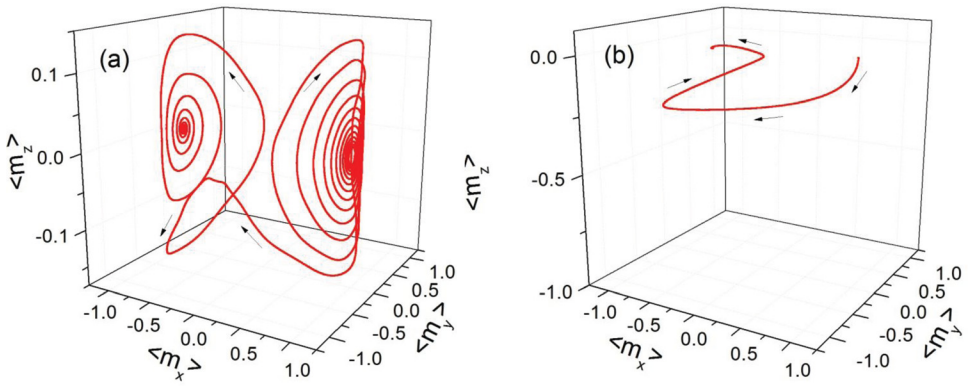

FIG. 3. Micromagnetic simulation results of the trajectories of the S and N states at $\beta = 10^{\circ}$ and (a) $J = 0.2 \times 10^8$ A/cm^2, (b) $J = 2 \times 10^8$ A/cm^2.

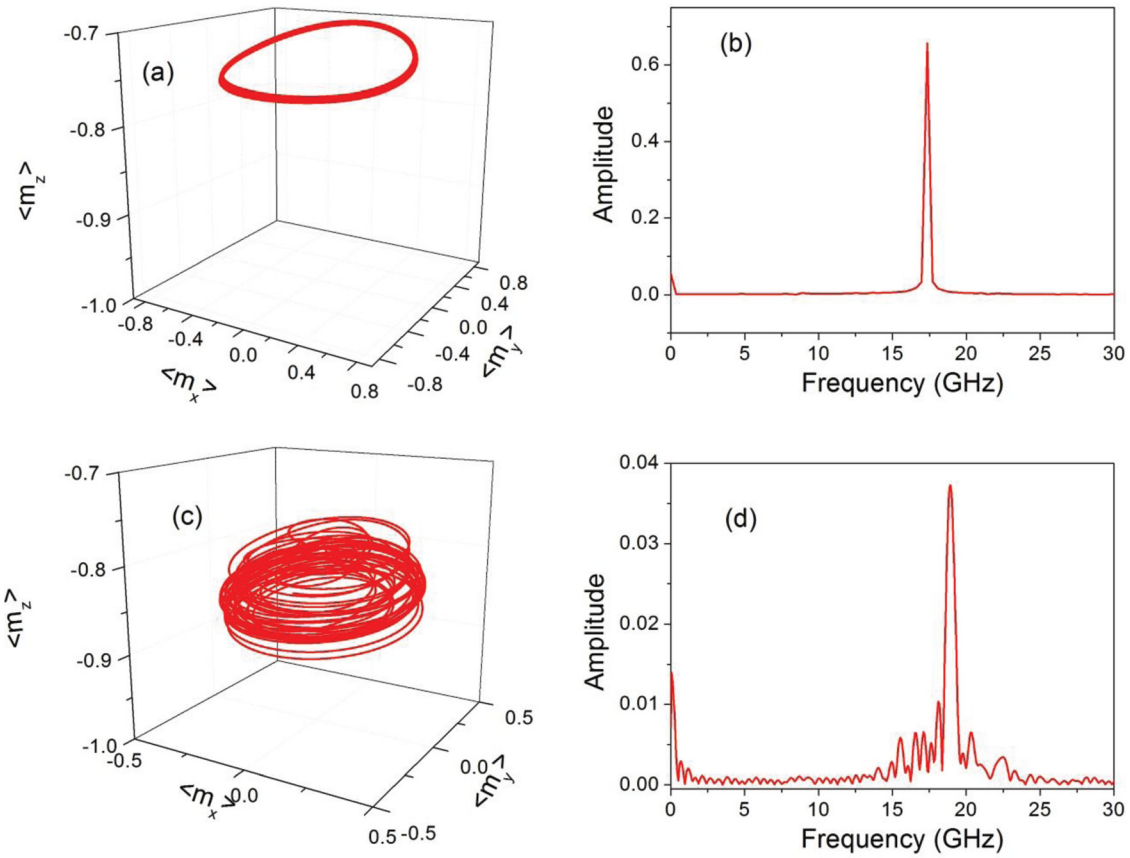

FIG. 4. Average magnetization precession of the L states by micromagnetic simulation at (a) $\beta = 10^{\circ}$, $J = 0.7 \times 10^8$ A/cm^2, and (c) $\beta = 10^{\circ}$, $J = 0.9 \times 10^8$ A/cm^2. The corresponding frequency spectra are shown in (b) and (d), respectively.

J, we find that the periodic precession of the L state loses stability and transforms into a spiral state along the $-z$ direction. A typical precession trajectory of the transient state between the L state and spiral state is given in Fig. 4(c). The back-and-forth precession in the z direction of the averaged magnetization is caused by the incoherent oscillations of the local magnetization of the free layer, which cannot be observed in the macrospin model. Correspondingly, some small chaotic peaks appear in the frequency spectrum, as shown in Fig. 4(d).

The dependence of the frequency on the current and tilt angle ($\beta \leq 30^{\circ}$) for the L precession state around the z-axis is summarized in Fig. 5. An obvious feature is that the current-dependence of the precession frequency is asymmetrical. Another interesting feature in Fig. 5 is that the frequency for the positive current increases from a few GHz to 20 GHz as the current increases. The frequency region narrows slightly when the tilt angle β of the polarizer increases. In contrast, for the negative current the frequency of the precession state barely changes, giving $f \sim 16$ GHz, as shown in the left panel of Fig. 5. We have compared the micromagnetic results in Fig. 5 to the analytical results in Fig. 1 and macrospin simulations in our earlier study.[34] Some noticeable differences will be: (1) the maximum oscillation frequency in single domain approximation is larger than that of micromagnetic simulations, and (2) micromagnetics simulations show strong asymmetry in the bias current dependence of frequency and the threshold current to excite the oscillation. These can be qualitatively understood by considering the following possible factors: (1) the micromagnetics simulations have taken the

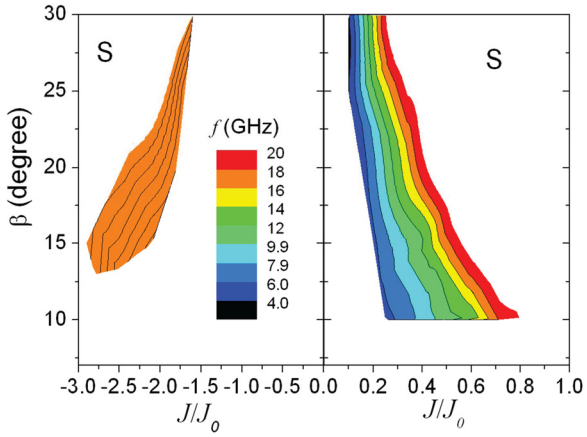

FIG. 5. Precession frequency dependence on the current density J and the tilt angle β.

spatial non-uniform distribution of magnetization into account. The higher order magnetization dynamics may be important in determining the effective anisotropy and thus the average magnetization precession frequencies.[59] (2) The strong asymmetry in the dependence of TP-STNO oscillation frequency on bias current for different current polarity may be due to the different spin-torque strength, which is strongly associated with the current polarity for the TP-STNO. In the positive current case, the spin torque enlarges the magnetization angle between the free layer and the polarizing layer while in the case of negative current, the magnetization angle between the two layers is relatively small. Therefore, for the same damping torque the spin torque requires larger current for the negative current direction than for the positive current direction, in order to reach the same frequency of steady-state precession. Furthermore, micromagnetic simulations show that for the negative current the averaged $\langle m_z \rangle$ of L-precession state is almost independent of current strength and β [not shown]. In contrast, for the positive current, the $\langle m_z \rangle$ decreases with the increasing of the current. Since the oscillation frequency is proportional to the z component of magnetization, i.e., $f \approx 4\pi m_z$, the asymmetrical $\langle m_z \rangle$ for different current polarity will result in the asymmetry in current dependence of frequency and can qualitatively explain the blue-shift of the frequency for positive current.

IV. CONCLUSION

We have shown by means of eigenvalue calculations and magnetodynamical simulations that a spintronic device with a tilted fixed-layer magnetization possesses a surprisingly rich phase diagram of static and dynamic states in a zero magnetic field. We have also examined the effects of the most important and most typical material parameters, including the saturation magnetization M_s and the damping coefficient α, on the phase diagram of the TP device. Such systematic studies provide experimentalists with a much deeper understanding of device characteristics and with useful guidelines for determining the optimal experimental and material parameter space for achieving the desired device properties. More importantly, a full-scale micromagnetics simulation has been performed for such system for the first time here, and it gives results that are quantitatively similar to those of our nonlinear theory and macrospin model, confirming the validity of our theory over a wide range of material parameters.

ACKNOWLEDGMENTS

Y. Zhou was supported by the Seed Funding for Fundamental Research of The University of Hong Kong (Project No. 106053). Johan Åkerman gratefully acknowledges financial support from The Swedish Foundation for Strategic Research (SSF), The Swedish Research Council (VR), the Göran Gustafsson Foundation, the Knut and Alice Wallenberg Foundation. Y. Liu thanks the supports from the NSFC (No. 10974142 and No. 11274241), Shuguang Program (No. 09SG22), and NCET (No. 10-0603).

[1]J. A. Katine, F. J. Albert, R. A. Buhrman, E. B. Myers, and D. C. Ralph, Phys. Rev. Lett. **84**, 3149 (2000).
[2]D. C. Ralph and M. D. Stiles, J. Magn. Magn. Mater. **321**, 2508 (2009).
[3]M. R. Pufall, W. H. Rippard, S. Kaka, T. J. Silva, and S. E. Russek, Appl. Phys. Lett. **86**, 082506 (2005).
[4]T. J. Silva and W. H. Rippard, J. Magn. Magn. Mater. **320**, 1260 (2008).
[5]Y. Zhou, J. Persson, S. Bonetti, and J. Akerman, Appl. Phys. Lett. **92**, 092505 (2008).
[6]Y. Zhou and J. Akerman, Appl. Phys. Lett. **94**, 112503 (2009).
[7]S. Bonetti, P. Muduli, F. Mancoff, and J. Akerman, Appl. Phys. Lett. **94**, 102507 (2009).
[8]P. K. Muduli, Y. Pogoryelov, S. Bonetti, G. Consolo, F. Mancoff, and J. Akerman, Phys. Rev. B **81**, 140408 (2010).
[9]P. K. Muduli, Y. Pogoryelov, Y. Zhou, F. Mancoff, and J. Akerman, Integr. Ferroelectr. **125**, 147 (2011).
[10]P. K. Muduli, Y. Pogoryelov, F. Mancoff, and J. Akerman, IEEE Trans. Magn. **47**, 1575 (2011).
[11]J. Akerman, Science **308**, 508 (2005).
[12]B. N. Engel, J. Akerman, B. Butcher, R. W. Dave, M. DeHerrera, M. Durlam, G. Grynkewich, J. Janesky, S. V. Pietambaram, N. D. Rizzo *et al.*, IEEE Trans. Magn. **41**, 132 (2005).
[13]A. M. Deac, A. Fukushima, H. Kubota, H. Maehara, Y. Suzuki, S. Yuasa, Y. Nagamine, K. Tsunekawa, D. D. Djayaprawira, and N. Watanabe, Nat. Phys. **4**, 803 (2008).
[14]A. V. Nazarov, K. Nikolaev, Z. Gao, H. Cho, and D. Song, J. Appl. Phys. **103**, 07A503 (2008).
[15]J. Grollier, V. Cros, and A. Fert, Phys. Rev. B **73**, 060409(R) (2006).
[16]Y. Zhou, J. Persson, and J. Akerman, J. Appl. Phys. **101**, 09A510 (2007).
[17]J. Persson, Y. Zhou, and J. Akerman, J. Appl. Phys. **101**, 09A503 (2007).
[18]D. Li, Y. Zhou, C. Zhou, and B. Hu, Phys. Rev. B **83**, 174424 (2011).
[19]D. Li, Y. Zhou, C. Zhou, and B. Hu, Phys. Rev. B **82**, 140407(R) (2010).
[20]D. Li, Y. Zhou, B. Hu, and C. Zhou, Phys. Rev. B **84**, 104414 (2011).
[21]Y. Zhou, V. Tiberkevich, G. Consolo, E. Iacocca, B. Azzerboni, A. Slavin, and J. Akerman, Phys. Rev. B **82**, 012408 (2010).
[22]D. Houssameddine, U. Ebels, B. Delaet, B. Rodmacq, I. Firastrau, F. Ponthenier, M. Brunet, C. Thirion, J.-P. Michel, L. Prejbeanu-Buda *et al.*, Nat. Mater. **6**, 447 (2007).
[23]W. H. Rippard, A. M. Deac, M. R. Pufall, J. M. Shaw, M. W. Keller, S. E. Russek, G. E. W. Bauer, and C. Serpico, Phys. Rev. B **81**, 014426 (2010).
[24]S. M. Mohseni, S. R. Sani, J. Persson, T. N. A. Nguyen, S. Chung, Y. Pogoryelov, and J. Akerman, Phys. Status Solidi (RRL) **5**, 432 (2011).
[25]V. S. Pribiag, I. N. Krivorotov, G. D. Fuchs, P. M. Braganca, O. Ozatay, J. C. Sankey, D. C. Ralph, and R. A. Buhrman, Nat. Phys. **3**, 498 (2007).
[26]V. S. Pribiag, G. Finocchio, B. J. Williams, D. C. Ralph, and R. A. Buhrman, Phys. Rev. B **80**, 180411 (2009).
[27]G. Finocchio, V. S. Pribiag, L. Torres, R. A. Buhrman, and B. Azzerboni, Appl. Phys. Lett. **96**, 102508 (2010).
[28]N. Locatelli, V. V. Naletov, J. Grollier, G. de Loubens, V. Cros, C. Deranlot, C. Ulysse, G. Faini, O. Klein, and A. Fert, Appl. Phys. Lett. **98**, 062501 (2011).
[29]A. Dussaux, A. V. Khvalkovskiy, J. Grollier, V. Cros, A. Fukushima, M. Konoto, H. Kubota, K. Yakushiji, S. Yuasa, K. Ando *et al.*, Appl. Phys. Lett. **98**, 132506 (2011).

[30]A. Dussaux, B. Georges, J. Grollier, V. Cros, A. V. Khvalkovskiy, A. Fukushima, M. Konoto, H. Kubota, K. Yakushiji, S. Yuasa *et al.*, Nat. Commun. **1**, 8 (2010).
[31]O. Boulle, V. Cros, J. Grollier, L. G. Pereira, C. Deranlot, F. Petroff, G. Faini, J. Barnas, and A. Fert, Nat. Phys. **3**, 492 (2007).
[32]Y. Zhou, C. L. Zha, S. Bonetti, J. Persson, and J. Akerman, J. Appl. Phys. **105**, 07D116 (2009).
[33]Y. Zhou, C. L. Zha, S. Bonetti, J. Persson, and J. Akerman, Appl. Phys. Lett. **92**, 262508 (2008).
[34]Y. Zhou, S. Bonetti, C. L. Zha, and J. Akerman, New J. Phys. **11**, 103028 (2009).
[35]R.-X. Wang, P.-B. He, Z.-D. Li, A.-L. Pan, and Q.-H. Liu, J. Appl. Phys. **109**, 033905 (2011).
[36]P.-B. He, Z.-D. Li, A.-L. Pan, Q.-L. Zhang, Q. Wan, R.-X. Wang, Y.-G. Wang, W.-M. Liu, and B.-S. Zou, J. Appl. Phys. **105**, 043908 (2009).
[37]P.-B. He, R.-X. Wang, Z.-D. Li, W.-M. Liu, A.-L. Pan, Y.-G. Wang, and B.-S. Zou, Eur. Phys. J. B **73**, 417 (2010).
[38]C. L. Zha, Y. Y. Fang, J. Nogues, and J. Akerman, J. Appl. Phys. **106**, 053909 (2009).
[39]C. L. Zha, J. Persson, S. Bonetti, Y. Y. Fang, and J. Akerman, Appl. Phys. Lett. **94**, 163108 (2009).
[40]C. L. Zha, S. Bonetti, J. Persson, Y. Zhou, and J. Akerman, J. Appl. Phys. **105**, 07E910 (2009).
[41]T. N. A. Nguyen, Y. Fang, V. Fallahi, N. Benatmane, S. M. Mohseni, R. K. Dumas, and J. Akerman, Appl. Phys. Lett. **98**, 172502 (2011).
[42]T. N. Anh Nguyen, N. Benatmane, V. Fallahi, Yeyu Fang, S. M. Mohseni, R. K. Dumas, Johan Åkerman, J. Magn. Magn. Mat. **324**, 3929 (2012).
[43]C.-M. Lee, J.-S. Yang, and T.-H. Wu, IEEE Trans. Magn. **47**, 649 (2011).
[44]R. Law, E.-L. Tan, R. Sbiaa, T. Liew, and T. C. Chong, Appl. Phys. Lett. **94**, 062516 (2009).
[45]S.-W. Lee and K.-J. Lee, IEEE Trans. Magn. **46**, 2349 (2010).
[46]M. Carpentieri, E. Martinez, and G. Finocchio, J. Appl. Phys. **110**, 093911 (2011).
[47]J. C. Slonczewski, J. Magn. Magn. Mater. **159**, L1 (1996).
[48]L. Berger, Phys. Rev. B **54**, 9353 (1996).
[49]Y. B. Bazaliy, B. A. Jones, and S. C. Zhang, Phys. Rev. B **69**, 094421 (2004).
[50]H. K. Khalil, *Nonlinear Systems*, 3rd ed. (Prentice-Hall, Upper Saddle River, NJ, 2002).
[51]J. H. Hubbard and B. H. West, *Differential Equations: A Dynamical Systems Approach* (Springer, Berlin, 1995).
[52]L. Perko, *Differential Equations and Dynamical Systems* (Springer, Berlin, 1996).
[53]G. Bertotti, C. Serpico, I. D. Mayergoyz, A. Magni, M. d'Aquino, and R. Bonin, Phys. Rev. Lett. **94**, 127206 (2005).
[54]X. Chen, Z. Zhu, Y. Jing, S. Dong, and J.-M. Liu, Phys. Rev. B **76**, 054414 (2007).
[55]G. Bertotti, I. D. Mayergoyz, and C. Serpico, *Nonlinear Magnetization Dynamics in Nanosystems* (Elsevier, New York, 2009).
[56]Y. B. Bazaliy, Phys. Rev. B **85**, 014431 (2012).
[57]W. Zhu, Y. Liu, and C.-G. Duan, Appl. Phys. Lett. **99**, 032508 (2011).
[58]W. Jin, Y. W. Liu, and H. Chen, IEEE Trans. Magn. **42**, 2682 (2006).
[59]Y. Zhou, J. Akerman, and J. Z. Sun, Appl. Phys. Lett. **98**, 102501 (2011).